Radiology

ORIGINAL RESEARCH ■ TECHNICAL DEVELOPMENTS

Comparison of Standard and Quadruple-Phase Contrast Material Injection for Artifacts, Image Quality, and Radiation Dose in the Evaluation of Head and Neck Cancer Metastases[1]

Charbel Saade, PhD
Fadi El-Merhi, MD, ABR
Ahmad Mayat, MD, FRANZCR
Patrick C. Brennan, PhD
David Yousem, MD, ABR

Purpose: To investigate opacification of head and neck vasculature during computed tomography (CT) of supraclavicular lymph nodes with a quadruple-phase contrast media and saline dual-injection protocol.

Materials and Methods: This retrospective study was institutional review board approved. In 180 consecutive patients, routine head and neck CT was performed with one of two protocols: protocol A, craniocaudal scan direction with 100 mL of contrast material injected intravenously as a single bolus; or protocol B, 100 mL of contrast material injected in four phases (phases 1–2, 60 mL of contrast material and saline injected at 2.5 mL/sec; phases 3–4, 40 mL of contrast material and saline injected at 2.5 mL/sec); both protocols had a fixed scan delay of 70 seconds. Attenuation of supraclavicular arteries and veins was measured with arteriovenous contrast ratio (AVCR) and contrast-to-noise ratio (CNR). Effective dose was calculated. Data were compared with the two-sample *t* test. Receiver operating characteristic (ROC) and visual grading characteristic analyses were performed.

Results: Arterial attenuation was up to 20% higher ($P < .05$) after protocol B (mean ± standard deviation, 234.5 HU ± 33.2) than protocol A (160.0 HU ± 29.5). Venous system attenuation was significantly lower in protocol B (164.0 HU ± 17.0) than in protocol A (664.0 HU ± 12.0), with up to a 75% reduction ($P < .0001$). Protocol B generated significant ($P < .0001$) improvements in AVCR at multiple anatomic sites. At all anatomic levels, mean CNR with protocol B (34.4 HU ± 9.0) was significantly higher than that with protocol A (14.5 HU ± 14.0) ($P < .0313$). Effective dose was significantly reduced with protocol B (2.6 mSv ± 0.4 vs 3.2 mSv ± 0.8 with protocol A; $P < .0041$). ROC analysis demonstrated significantly higher area under the ROC curve for protocol B ($P < .0022$), with interreader agreement increasing from poor to excellent in lymph node visualization.

Conclusion: Significant improvement in lymph node visualization at the cervicothoracic junction is achieved with a quadruple-phase contrast media injection protocol.

©RSNA, 2015

[1] From the Department of Diagnostic Radiology, American University of Beirut Medical Center, PO Box 11-0236, Riad El Solh, Beirut 1107 2020, Lebanon (C.S., F.E.); Department of Radiology, Campbelltown Public Hospital, Campbelltown, NSW, Australia (A.M.); Discipline of Medical Radiation Sciences, University of Sydney, Lidcombe, NSW, Australia (P.C.B.); and Department of Diagnostic Radiology, Johns Hopkins Hospital, Baltimore, Md (D.Y.). Received March 2, 2015; revision requested May 6; revision received July 6; accepted July 17; final version accepted August 27. **Address correspondence to** F.E. (e-mail: *fe19@aub.edu.lb*).

Computed tomographic (CT) images of the head and neck frequently contain artifacts that reflect the limitations in contrast media delivery. Perivenous artifacts caused by the inflow of high contrast media volumes into the brachiocephalic vein (BCV) and superior vena cava or by retrograde filling from the superior vena cava into the BCV during CT of the head and neck are a well-reported concern during the evaluation of supraclavicular adenopathy (1–6). The aim of this study was to examine opacification of the head and neck vasculature at CT and the detection of cervicothoracic junction lymph nodes in patients with head and neck cancer by using a quadruple-phase contrast material injection protocol.

Materials and Methods

Study Population

The institutional review board approved this retrospective study, and written informed consent was waived, since all studies were clinically indicated and patient data were evaluated anonymously. Patients were referred from the oncology department with known squamous cell carcinoma of the neck between November 2012 and May 2013. Ninety consecutive patients underwent the conventional imaging protocol (protocol A) and surgical nodal resection as the baseline condition. Between June 2013 and January 2014, 90 consecutive patients underwent the quadruple-phase contrast material injection protocol (protocol B) and surgical nodal resection. The analysis was conducted to compare radiologic findings and histopathologic results. There were no exclusion criteria used in the study, since all patients who were evaluated underwent imaging and surgical resection.

Head and Neck CT Acquisition

All examinations were performed by using a 256-section multidetector CT scanner (Philips iCT; Philips Healthcare, Best, the Netherlands). The scanning range was from the aortopulmonary window to the frontal sinus. CT scanning parameters used in each protocol were detector width of 256 × 0.625 mm; pitch of 0.881:1 ratio; rotation time of 0.27 seconds; 120 kVp; 120 mA with x-, y-, and z-axis modulation; and iterative reconstruction (iDose[4]; Philips).

Contrast Material Bolus Geometry

Contrast media (Optiray, 370 mg/L; Mallinckrodt, Cincinnati, Ohio) and a saline chaser were injected with an automated dual-barrel power injector (Optivantage; Mallinckrodt) via a 20-gauge venous catheter in the right antecubital vein, since it provides the shortest contrast media route with the least amount of dilution (7). Protocol A consisted of administration of 100 mL of contrast media, followed by 100 mL of saline at a flow rate of 2.5 mL/sec with a fixed scan delay of 70 seconds. The volume of contrast media was not tailored to the patient's body mass index (8) but was in line with volumes given in the current literature (9). With protocol B, the quadruple-phase technique was used: 60 mL of contrast material and saline were injected, followed by 40 mL of contrast material and saline with an injection rate of 2.5 mL/sec in each phase. Protocol B also had a fixed scan delay of 70 seconds.

Attenuation Measurements

Attenuation in Hounsfield units was measured by an expert in CT and magnetic resonance (MR) imaging (C.S., with 15 years of experience) in the axial plane within a circular region of interest (ROI) diameter that fitted within the lumen of the vessel. The mean and standard deviation within the ROI in each vessel were recorded. Arterial measurements occurred at six anatomic locations, resulting in 20 measurements at each level, on the left and right sides: *(a)* middle cerebellar and basilar (at the level of suprasellar cistern) distal internal carotid artery and vertebral arteries (at the level of the foramen magnum and foramen ovale); *(b)* origin of the internal carotid artery, *(c)* middle segments of the vertebral artery (fourth cervical vertebral level); *(d)* proximal (suprasellar cistern) and distal (fourth cervical vertebra) external carotid artery; *(e)* middle segments of the common carotid artery (at the level of the hyoid bone); and *(f)* origin of the vertebral artery (level of the sternal notch) and ascending aorta (third thoracic vertebral level) (Fig 1).

Attenuation values in veins adjacent to the arteries and at the same anatomic levels as the arteries were documented: transverse sinus (at the level of the suprasellar cistern); cranial internal jugular vein (at the level of the foramen magnum and foramen ovale); middle division of the internal jugular vein (just beyond the carotid bifurcation

Advances in Knowledge

- Split-bolus contrast media delivery reduces arterial and venous opacification artifacts in the cervicothoracic junction by 75% (mean ± standard deviation, 164 HU ± 12; $P < .0001$).
- Uniform opacification between cervical arteries and veins increases the delineation between vessels and lymph nodes (95% confidence interval: 0.98, 1.0) when using a quadruple-phase contrast material injection protocol ($P < .0022$).
- Uniform distribution of contrast media reduces effective radiation dose in the head and neck by 19% (2.6 mSv ± 0.4).

Published online before print
10.1148/radiol.2015150511 **Content codes:** CT HN

Radiology 2016; 279:571–577

Abbreviations:
AVCR = arteriovenous contrast ratio
BCV = brachiocephalic vein
CNR = contrast-to-noise ratio
ROC = receiver operating characteristic
ROI = region of interest

Author contributions:
Guarantor of integrity of entire study, C.S.; study concepts/study design or data acquisition or data analysis/interpretation, all authors; manuscript drafting or manuscript revision for important intellectual content, all authors; approval of final version of submitted manuscript, all authors; agrees to ensure any questions related to the work are appropriately resolved, all authors; literature research, all authors; clinical studies, C.S., F.E., A.M.; experimental studies, C.S., A.M.; statistical analysis, C.S., A.M.; and manuscript editing, C.S., F.E., A.M., D.Y.

Conflicts of interest are listed at the end of this article.

Figure 1

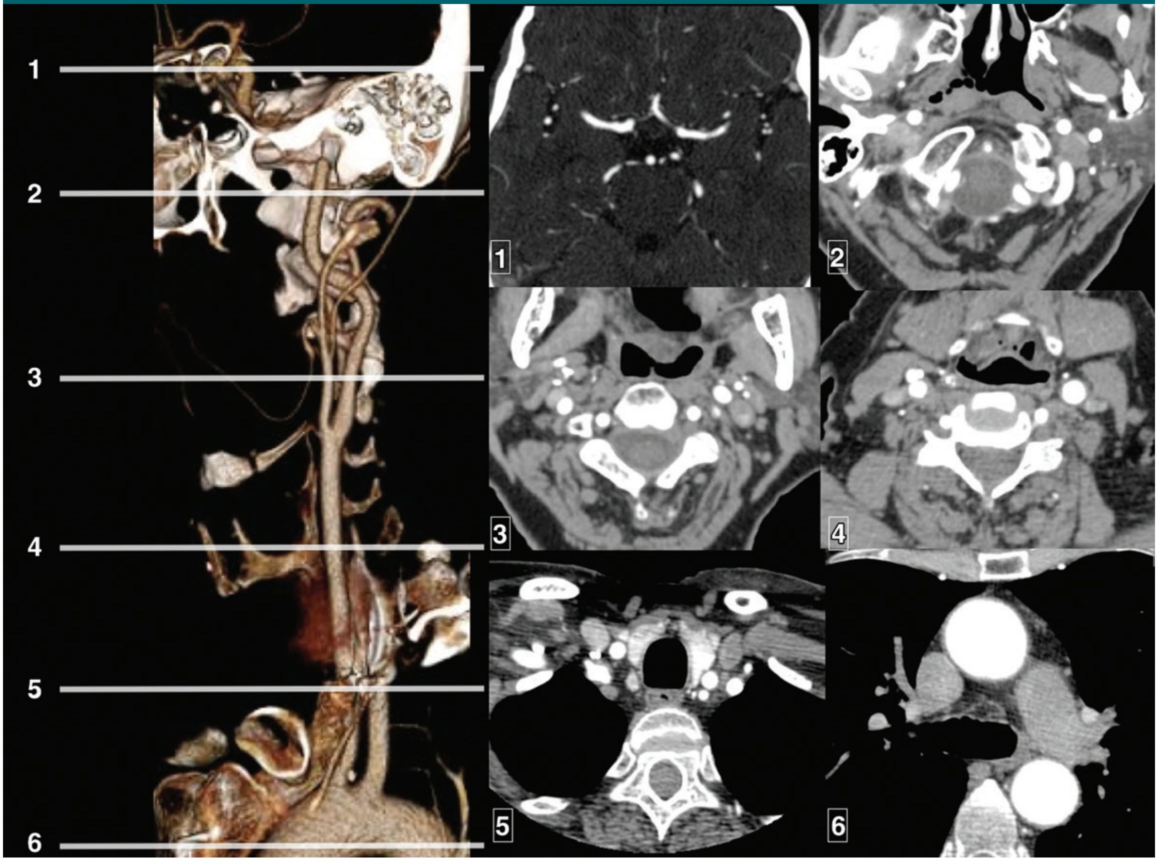

Figure 1: Sagittal three-dimensional volume-rendered CT image (left) and axial CT images (right) show the anatomic location and measurements of the head and neck vasculature.

at the level of the fourth cervical vertebra); caudal division of the internal jugular vein (at the level of the hyoid bone); right BCV (at the sternal notch level); and superior vena cava (at the third thoracic vertebra level). The degree of contrast between arteries and veins was conveyed as a ratio of CT values in Hounsfield units (arteries to veins) at each anatomic level and described as the arteriovenous contrast ratio (AVCR). At each level of multiple arteries and veins, values in each vessel group were averaged.

Contrast-to-Noise Ratio Measurement

Contrast-to-noise ratio (CNR) analysis was conducted by using a 3-mm-thick transaxial image. The ROI was drawn as large as the vessel lumen diameter permitted, carefully avoiding calcified and/or soft plaques of the vessel wall. When calculating the CNR, the attenuation of the right sternocleomastoid muscle (ROI_{SCM} in the following equation) was measured at the level of the fourth cervical vertebra, followed by the second measurement of noise as the standard deviation in the foam mattress of the CT gantry. To compare the overall degree of vascular opacification within the entire head and neck vasculature, the mean opacification for each patient was measured below the carotid bifurcation (ROI_{CF} in the following equation). The CNR was calculated on the basis of the measured parameters described earlier, with an empirically derived formula: CNR = $(\mathrm{ROI}_{\mathrm{CF}} - \mathrm{ROI}_{\mathrm{SCM}})$/noise.

Radiation Dose Measurement

The effective dose (in millisieverts), dose-length product (in milligray centimeters), and CT dose index were calculated and recorded from the patient dose report. A normalized conversion factor (k[effective dose/dose-length product]), for the neck—0.0054 mSv/mGy · cm—was used to calculate the effective dose (10): effective dose = dose-length product × k.

Image Assessment

Transaxial images (0.625-mm section thickness, 0.5-mm increment) obtained by using a smooth convolution kernel (field of view, 380 × 380 mm; image matrix, 512 × 512) were assessed on a reporting workstation (IMPAX 6.3.1; Agfa, Mortsel, Belgium) with a gray-scale standard display function–calibrated 3-megapixel monitor. Attenuation measurements, receiver operating characteristic (ROC) analysis for lymph node

Table 1

Mean Attenuation of Arteries and Veins in Each Anatomic Segment during Head and Neck CT

Anatomic Level and Location	Attenuation with Protocol A (HU)	Attenuation with Protocol B (HU)	*P* Value
Arterial			
Suprasellar cistern			
RMCA	148 ± 36	216 ± 30	<.0013
RECA–ST	159 ± 46	199 ± 40	<.0013
LECA–ST	150 ± 23	234 ± 33	<.0013
LMCA	162 ± 38	218 ± 42	<.0013
Basilar artery	173 ± 16	220 ± 38	<.0012
Foramen magnum			
RICA–FO	166 ± 27	236 ± 29	<.0011
RVA-FM	152 ± 32	232 ± 36	<.0013
LICA–FO	177 ± 29	256 ± 44	<.0013
LVA-FM	169 ± 44	275 ± 39	<.0013
Hyoid bone			
RCC	160 ± 41	274 ± 32	<.0013
LCC	172 ± 53	260 ± 61	<.0011
Sternal notch			
RVA–origin	151 ± 22	216 ± 33	<.0012
LVA–origin	149 ± 44	199 ± 43	<.0013
Fourth cervical vertebra			
RICA–origin	150 ± 21	234 ± 41	<.0012
RECA–origin	162 ± 31	218 ± 33	<.0012
RVA–C4	143 ± 19	220 ± 38	<.0011
LICA–origin	166 ± 29	236 ± 36	<.0011
LECA–origin	162 ± 19	232 ± 29	<.0012
LVA–C4	157 ± 31	256 ± 37	<.0012
Third thoracic vertebra			
Ascending aorta	169 ± 44	265 ± 58	<.0012
Venous			
Suprasellar cistern			
T-sinus	229 ± 144	169 ± 18	<.0001
Foramen magnum			
IJV–JF	213 ± 136	164 ± 12	<.0001
Fourth cervical vertebra			
IJV–C4	217 ± 138	167 ± 28	<.0001
Hyoid bone			
IJV–proximal	217 ± 138	165 ± 17	<.0001
Sternal notch			
BCV	659.8 ± 19	181 ± 19	<.0001
Third thoracic vertebra			
Superior vena cava	664.5 ± 12	199 ± 22	<.0001

Note.—Data are means ± standard deviations, unless indicated otherwise. C4 = fourth cervical vertebra, FO = foramen ovale, FM = foramen magnum, IJV = internal jugular vein, JF = jugular foramen, LCC = left common carotid artery, LECA = left external carotid artery, LICA = left internal carotid artery, LMCA = M1 portion of the left middle cerebral artery, LVA = left vertebral artery, RCC = right common carotid artery, RECA = right external carotid artery, RICA = right internal carotid artery, RMCA = M1 portion of the right middle cerebral artery, RVA = right vertebral artery, ST = superficial temporal artery, T-sinus = transverse sinus.

detection, and visual grading characteristic methods were used to evaluate contrast media filling at the cervicothoracic junction.

ROC Analysis

For each protocol and scanning technique, 40 complete cases were randomly chosen, with an equal number of normal and abnormal cases, totaling 80 cases. Such cases showed lymphadenopathy of varying degrees as defined by two radiologists' reports (based on complete patient case series, with previous and subsequent examination findings included). The ordering of image viewing was performed in a counterbalanced way: clinician 1 (F.E., with 19 years of experience) looked at images obtained with protocol A first and then those obtained with protocol B, and clinician 2 (A.M., with 18 years of experience) looked at images obtained with protocol B first and then images obtained with sprotocol A, and so on.

Two neuroradiologists (F.E., A.M.) who had been certified by the American Board of Radiology and the Royal Australian and New Zealand College of Radiologists and had a mean of 14 years of experience assessed the images. Observers were allowed to manipulate the window width and level of the images. Each image in the first sitting was presented, and a score of 1–6 was assigned, where 6 indicated that lymph node pathologic abnormalities were present, and 1 represented that abnormalities were not present.

Visual Grading Analysis

The visual grading characteristic method (11) was used to illustrate viewer preference of one technique over another, based on the visibility of lymph node distribution. Specifically for this work, the presence of lymph nodes was indicated by using a four-point visualization classification scale, where 0 indicated poor visualization, 1 indicated less than 50% visualization, 2 indicated more than 50% visualization, and 3 indicated visualization of all lymph nodes at the cervicothoracic junction.

Statistical Analysis

Two-sample t tests were used to compare patient sex, age, height, weight, body mass index, effective dose, scanning time, scanning range, and measured opacity values between the two patient groups. The ROC analyses were performed with the Dorfman-Berbaum-Metz approach by using readers as random variables and cases as fixed variables (12). Cases were treated as fixed variables on the basis of the fact that the limited image sample size was not taken as a representation of all images. Results were considered to indicate a statistically significant difference if the *P* value was less than .05. Inter- and intraobserver agreements were calculated by using Cohen κ analysis. A κ value of 0.61–1.0, 0.41–0.60, 0.21–0.40, and less than 0.20 were considered to indicate excellent, moderate, fair, and poor agreement, respectively.

Results

Patient Demographics, CT Acquisition, and Radiation Dose

There was no significant difference in patient sex, age, height, weight, or body mass index between the two protocols ($P \geq .05$). The effective dose was significantly reduced with protocol B (mean ± standard deviation, 3.2 mSv ± 0.8 for protocol A and 2.6 mSv ± 0.4 for protocol B; $P < .0041$). There was no significant difference in mean scanning time (in seconds) in protocol B (3.22 seconds ± 1.2) compared with protocol A (3.01 seconds ± 1.3, $P = .83$) or in scanning range (in centimeters) for each protocol (protocol A, 33.2 cm ± 2.01; and protocol B, 32.9 cm ± 3.03; $P = .83$).

Opacification of the Head and Neck Vasculature and CNR

Mean arterial opacification (in Hounsfield units) in the arteries measured was 20% higher in protocol B (275 HU ± 39) compared with A (148 HU ± 36) ($P < .0013$) (Table 1). Attenuation in the veins was significantly lower in protocol B (164 HU ± 17) than in protocol A (664 HU ± 12), with a maximum reduction equal to 75% ($P < .0001$) (Table 1). Protocol B showed significant ($P < .0001$) improvements in AVCR at a variety of anatomic sites (Table 2). At all anatomic levels, the mean CNR for protocol B was significantly higher than that for protocol A (protocol B, 34.4 HU ± 9.0; protocol A, 14.5 HU ± 14.0; $P < .0313$).

Table 2

Mean Attenuation Profile of Arteries and Veins at Each Anatomic Level and AVCR Values

	Attenuation with Protocol A			Attenuation with Protocol B		
Anatomic Level	Arterial (HU)	Venous (HU)	AVCR	Arterial (HU)	Venous (HU)	AVCR
Suprasellar cistern	155	188	0.82	225	157	1.43
Foramen magnum	170	213	0.80	235	115	2.04
Fourth cervical vertebra	160	217	0.74	222	151	1.47
Hyoid bone	165	203	0.81	265	165	1.60
Sternal notch	168	659	0.25	266	181	1.46
Third thoracic vertebra	169	664	0.25	265	199	1.33

Figure 2

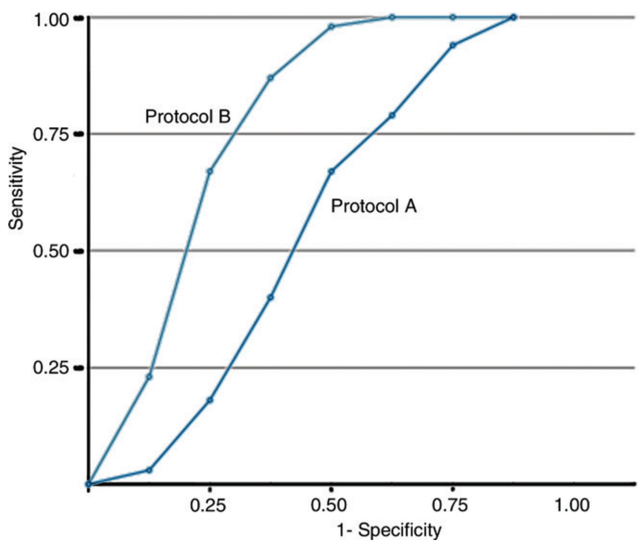

Figure 2: Visual grading characteristic curve. The circles represent the operating points corresponding to the scale steps of the rating scale. The graph represents protocol A compared with protocol B during head and neck CT by using the conventional protocol versus the quadruple-phase contrast material injection protocol.

Image Evaluation

Visual grading characteristic analysis.—The four-point scores individually graded by the two readers for each contrast media protocol were expressed as a graph shown in Figure 2. The graphs demonstrate that the area under the curve in protocol B (area under the curve, 0.91) was preferred to that of protocol A (area under the curve, 0.79).

ROC analysis.—The six-point scale demonstrated a significant difference between protocols, with mean ROC values demonstrating increased reader confidence range with protocol B (95% confidence interval: 0.98, 1.0) compared protocol with A (95% confidence interval: 0.78, 0.88) ($P < .0022$). Head and neck CT yielded excellent ($P < .03$) interobserver agreement with protocol B (k = 0.73) compared with protocol A (k = 0.51), and there was a strong positive relationship between vascular opacification and reader confidence in protocol B over protocol A ($r = 0.55$, $P < .0014$).

Figure 3

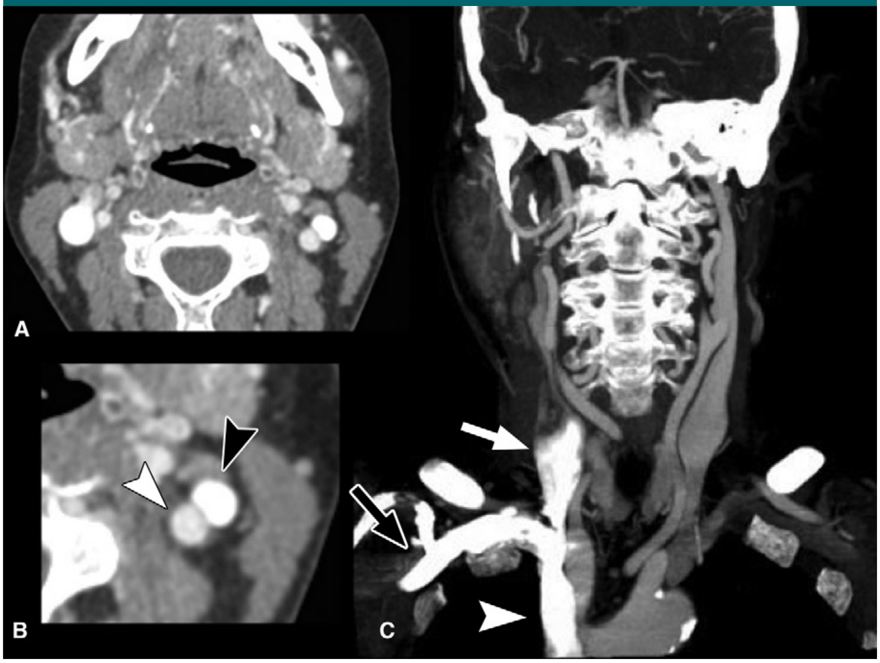

Figure 3: CT images of the neck in a 47-year-old woman, obtained with the dual-phase method, demonstrate perivenous artifacts that interfere with image interpretation. *A, B,* Axial images demonstrate reduced AVCR between the internal carotid artery (black arrowhead on *B*) and internal jugular vein (white arrowhead on *B*). *C,* Coronal image shows contrast material reflux into the internal jugular vein (white arrow), BCV (black arrow), and superior vena cava (arrowhead), obscuring evaluation of the vertebral arteries.

Figure 4

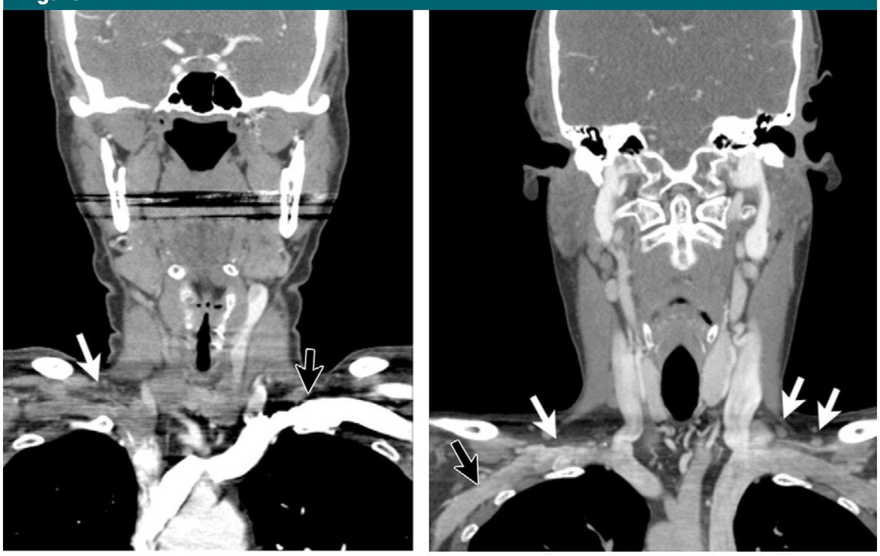

a. b.

Figure 4: **(a)** Coronal CT image obtained in the neck of a 63-year-old woman. The incoming redundant contrast material (black arrow) was scanned 70 seconds after injection, with poor visualization of the lymph nodes (white arrow) in the cervicothoracic junction. **(b)** Coronal CT image obtained in the neck of a 58-year-old man. The quadruple-phase contrast material technique was used, where complete visualization of the lymph nodes (white arrows) is shown because there is complete washout of redundant contrast material in the BCV (black arrow).

Final Diagnosis

In protocol A, final radiologic diagnoses included lymphadenopathy in 15 of 50 patients, with four necrotic nodes, including one node smaller than 10 mm and three nodes larger than 10 mm, with the remaining nodes having a normal appearance. Surgically, they were all confirmed with a discrepancy of six metastatic lymph nodes (two nodes $<$ 10 mm and four nodes $>$ 10 mm) that were not visualized during head and neck CT. In protocol B, malignant lymphadenopathy was present in 12 of 50 patients; with necrotic lymph nodes smaller than 10 mm in four of 50 and larger than 10 mm in eight of 50; the remaining nodes had a normal appearance. There was no surgical discrepancy with the radiology report.

Discussion

In the current study, we compared a novel quadruple-phase contrast material injection protocol with the conventional dual-phase protocol. We used a multiparametric model to perform the comparison, in which we considered attenuation levels within blood vessels, CNR, and ROC analysis with the overall aim of investigating the effect of the protocol on the diagnosis of metastatic lymph nodes in the cervicothoracic junction (Fig 3). The results were consistent: The novel approach clearly improved opacification of the artery and minimized opacification of the adjacent veins, thus potentially reducing vascular artifact and enhancing the CNR (Fig 4). These measurable features ultimately resulted in better diagnosis, where the expert neuroradiologists demonstrated higher ROC values with protocol B compared with protocol A, with no surgical discrepancies noted for the former. The consistency of the improvement with the quadruple-phase method over the conventional approach, regardless of the metric used, emphasizes the usefulness of our proposed technique.

Improved image quality with CT examinations comes at a cost, particularly with regard to radiation dose (13,14). This work demonstrates an exception, where the radiation dose was actually reduced. This dose savings offers substantial benefits to the examination, since radiation levels to the adjacent portions of the head and neck that are sensitive to radiation, such as the lens of the eye and the thyroid, are minimized. The interplay between radiation dose and contrast-enhanced protocol has often been overlooked, with the focus being on perivenous artifact reduction via patient-specific contrast material formulas during CT angiography (15–17), reduced x-ray tube voltage (14), contrast media with low iodine concentration, and iterative reconstruction (18), while attempting to maintain image quality (19). The current analysis highlights the value of quadruple-phase contrast media delivery that can reduce radiation dose to patients during head and neck CT while increasing image quality and reader confidence. It is difficult to draw precise comparisons with the literature, since the quadruple-phase approach for lymph node diagnosis at head and neck CT has not been used previously in head and neck imaging.

There are shortcomings in this study; the use of positron emission tomography (PET)/CT with histopathologic dissections could further clarify the diagnostic accuracy and surgical outcome on the basis of our contrast-enhanced protocol. Surgical results were only examined in the anatomic region of the lymph node that was being resected. We did not study the same patients with both protocols but had two different patient populations with different nodal findings. Therefore, predicting accurate clinical outcomes in regional and distant lymph node metastasis with our novel contrast media technique would ideally be confirmed with the use of PET/CT and histopathologic findings.

In summary, we present a quadruple-phase contrast media injection protocol that demonstrates significant improvements in the visualization of metastatic cervicothoracic lymph nodes during head and neck CT.

Disclosures of Conflicts of Interest: C.S. disclosed no relevant relationships. **F.E.** disclosed no relevant relationships. **A.M.** disclosed no relevant relationships. **P.C.B.** disclosed no relevant relationships. **D.Y.** disclosed no relevant relationships.

References

1. Chong V. Cervical lymphadenopathy: what radiologists need to know. Cancer Imaging 2004;4(2):116–120.

2. Saade C, Bourne R, El-Merhi F, Somanathan A, Chakraborty D, Brennan P. An optimised patient-specific approach to administration of contrast agent for CT pulmonary angiography. Eur Radiol 2013;23(11):3205–3212.

3. Saade C, Bourne R, Wilkinson M, Brennan PC. MDCT angiography of the major congenital anomalies of the extracranial arteries: pictorial review. J Med Imaging Radiat Oncol 2013;57(3):321–328.

4. Saade C, Bourne R, Wilkinson M, Evanoff M, Brennan P. A reduced contrast volume acquisition regimen based on cardiovascular dynamics improves visualisation of head and neck vasculature with carotid MDCT angiography. Eur J Radiol 2013;82(2):e64–e69.

5. Saade C, Bourne R, Wilkinson M, Evanoff M, Brennan PC. Caudocranial scan direction and patient-specific injection protocols optimize ECG-gated and non-gated thoracic CTA. J Comput Assist Tomogr 2013;37(5):725–731.

6. Saade C, Bourne R, Wilkinson M, Brennan P. Contrast medium administration and parameters affecting bolus geometry in multidetector computed tomography angiography: an overview. J Med Imaging Radiat Sci 2011;42(3):113–117.

7. You SY, Yoon DY, Choi CS, et al. Effects of right- versus left-arm injections of contrast material on computed tomography of the head and neck. J Comput Assist Tomogr 2007;31(5):677–681.

8. Nakaura T, Awai K, Yauaga Y, et al. Contrast injection protocols for coronary computed tomography angiography using a 64-detector scanner: comparison between patient weight-adjusted- and fixed iodine-dose protocols. Invest Radiol 2008;43(7):512–519.

9. Weininger M, Barraza JM, Kemper CA, Kalafut JF, Costello P, Schoepf UJ. Cardiothoracic CT angiography: current contrast medium delivery strategies. AJR Am J Roentgenol 2011;196(3):W260–W272.

10. Huda W, Ogden KM, Khorasani MR. Converting dose-length product to effective dose at CT. Radiology 2008;248(3):995–1003.

11. Båth M, Månsson LG. Visual grading characteristics (VGC) analysis: a non-parametric rank-invariant statistical method for image quality evaluation. Br J Radiol 2007;80(951):169–176.

12. Hillis SL, Berbaum KS, Metz CE. Recent developments in the Dorfman-Berbaum-Metz procedure for multireader ROC study analysis. Acad Radiol 2008;15(5):647–661.

13. Russell MT, Fink JR, Rebeles F, Kanal K, Ramos M, Anzai Y. Balancing radiation dose and image quality: clinical applications of neck volume CT. AJNR Am J Neuroradiol 2008;29(4):727–731.

14. May MS, Kramer MR, Eller A, et al. Automated tube voltage adaptation in head and neck computed tomography between 120 and 100 kV: effects on image quality and radiation dose. Neuroradiology 2014;56(9):797–803.

15. Saade C, Bourne R, El-Merhi F, Somanathan A, Chakraborty D, Brennan P. An optimised patient-specific approach to administration of contrast agent for CT pulmonary angiography. Eur Radiol 2013;23(11):3205–3212.

16. Saade C, Bourne R, Wilkinson M, Evanoff M, Brennan P. A reduced contrast volume acquisition regimen based on cardiovascular dynamics improves visualisation of head and neck vasculature with carotid MDCT angiography. Eur J Radiol 2013;82(2):e64–e69.

17. Saade C, Bourne R, Wilkinson M, Evanoff M, Brennan PC. Caudocranial scan direction and patient-specific injection protocols optimize ECG-gated and non-gated thoracic CTA. J Comput Assist Tomogr 2013;37(5):725–731.

18. Gaddikeri S, Andre JB, Benjert J, Hippe DS, Anzai Y. Impact of model-based iterative reconstruction on image quality of contrast-enhanced neck CT. AJNR Am J Neuroradiol 2015;36(2):391–396.

19. Yin WH, Lu B, Gao JB, et al. Effect of reduced x-ray tube voltage, low iodine concentration contrast medium, and sinogram-affirmed iterative reconstruction on image quality and radiation dose at coronary CT angiography: results of the prospective multicenter REALISE trial. J Cardiovasc Comput Tomogr 2015;9(3):215–224.